Chemical Science

ROYAL SOCIETY OF CHEMISTRY

EDGE ARTICLE

View Article Online
View Journal

Cite this: DOI: 10.1039/d6sc01535b

All publication charges for this article have been paid for by the Royal Society of Chemistry

Breaking the limit – synthesis and properties of *p*-amino-triazatriangulenium, the most stable carbenium ion

Marko H. Nowack, [a] Gennaro Pescitelli, [b] Arianna Lanza [a] and Bo W. Laursen *[a]

Received 23rd February 2026
Accepted 4th May 2026

DOI: 10.1039/d6sc01535b

rsc.li/chemical-science

Highly stabilized tris(dialkylamino)-triazatriangulenium (A-TATA$^+$) and tris(methoxy)-triazatriangulenium (MeO-TATA$^+$) carbenium ions have been synthesized and characterized as fluorescent dyes. As a result of the extensive delocalization of positive charge in the planar triangulenium system and the presence of six strongly electron-donating groups, these new carbenium ions display extreme cation stability. A linear correlation between cation stability (pK_{R+}) and reduction potential (E_{red}) has been established for the trianguleniums, leading to an estimated pK_{R+} value of 32 for A-TATA$^+$, making A-TATA$^+$ the most stable carbenium ion reported to date, surpassing the previous record by 7 pK_{R+} units. Furthermore A-TATA$^+$ displays unique dye properties in the blue spectral region, with intense absorption at 447 nm (ε = 84 000 cm^{-1} M^{-1}), and a high fluorescence quantum yield at 460 nm (ϕ_f = 45%).

Introduction

Stabilized carbenium ions such as triarylmethyliums, xantheniums, and acridiniums are organic compounds of great scientific and commercial importance.[3] They are extensively used as textile and laser dyes, and are prevalent among the brightest fluorescent probes and cellular stains used for bioimaging and assays.[4–6] The attractive spectral and photophysical properties of the carbenium ions originate from a conjugated π-system with an odd number of sp^2 centers that results in red-shifted spectra and high absorption coefficients in moderate-sized conjugated chromophore structures.[4,7–9] Spectral properties are readily tuned by position and electronegativity of substituents, such as the bridging group in rhodamine-type dyes.[10] This is highlighted by the pioneering work from several researchers on the diversification of the rhodamine scaffold, toward red-shifted fluorescent probes (Fig. 1a).[11–16] The cationic π-systems are in general electron deficient, which makes them strong one-electron acceptors in the excited state and thus useful as oxidative photocatalysts.[17–21] In particular, acridinium systems have found use for a multitude of oxidative photoredox catalyzed reactions (Fig. 1b). For these applications, tuning of the redox potentials is a key feature that is achieved by adding groups either stabilizing or destabilizing the carbenium system.[22–26] Stabilized carbenium ions have also seen applications in symmetrical organic redox flow batteries, where the excellent electrochemical stability makes them promising materials (Fig. 1c).[27–30] For this and other redox applications, the number and nature of donor atoms/groups (mainly O and N) controls the electron affinity of the carbenium ion and thus the redox potential.[31] It is not only the one-electron reduction/oxidation that is important for carbenium ions; nucleophilic addition of anions to the cationic dyes is also a key feature that leads to breaking of conjugation and formation of non-colored leuco adducts.[32–35] This feature has been explored *e.g.* in fluorogenic rhodamine probes switched on at low pH or by interactions with various analytes. Also, in this case tuning of the cation stability is a vital design parameter. For redox related applications, the relevant measure of cation stability is the reduction potential (E_{red}) while the cation stability towards nucleophiles is measured by the pK_{R+} value, that quantifies the equilibrium between a carbenium ion and the corresponding alcohol (carbinol) formed by addition of hydroxide ions.[36] The pK_{R+} values of carbenium ions have been extensively used to rank their stabilities, and are essential to evaluate reactivity towards nucleophiles, thus determining the operating conditions for dyes, probes, and catalysts.[1,31,37–40]

Stabilized carbenium ions owe their stability to the addition of electron-donating groups, delocalizing the positive charge. Historically (Fig. 1d), this has been accomplished either by *p*-functionalization, exemplified by crystal violet, or by *o*-fusion of neighboring aryl groups *via* heteroatom bridges, exemplified by the acridinium and TriOxaTriangulenium (TOTA$^+$) ions. The threefold bridging and extended conjugation of the triangulenium salts (Fig. 1d) make them among the most stable carbenium ions reported in the literature to date. The positive charge is delocalized onto the heterocyclic framework as

[a]Department of Chemistry, University of Copenhagen, Universitetsparken 5, 2100, Copenhagen Ø, Denmark. E-mail: bwl@chem.ku.dk

[b]Dipartimento di Chimica e Chimica Industriale, Università di Pisa, Via Giuseppe Moruzzi 13, 56124 Pisa, Italy

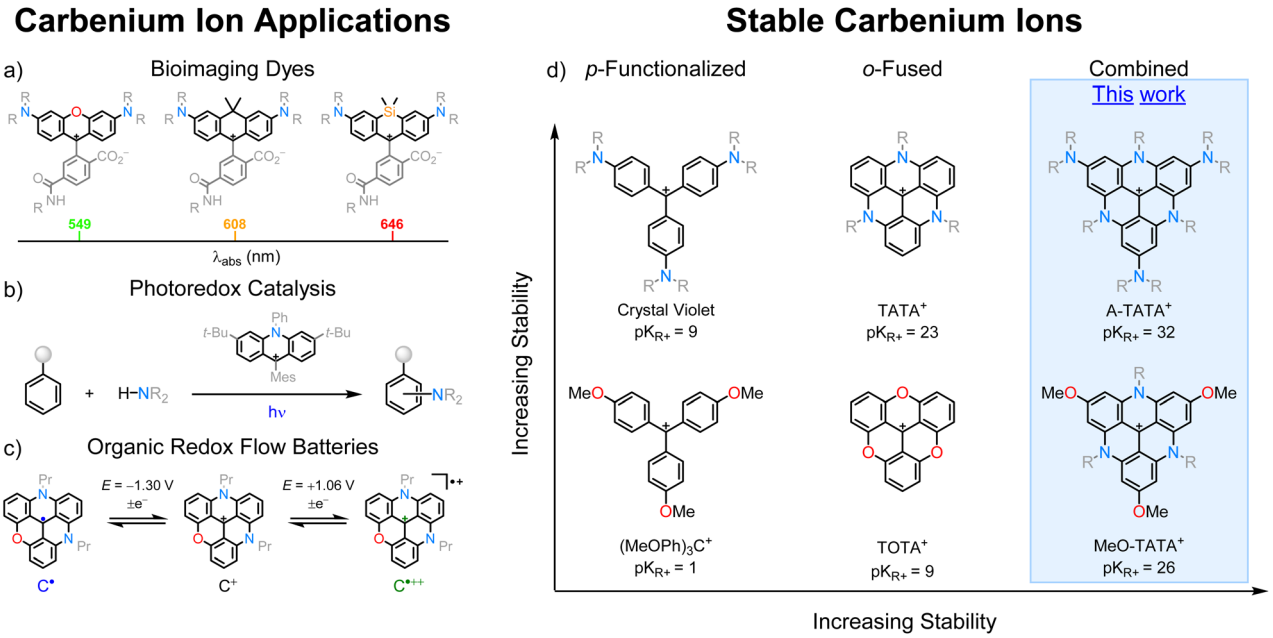

Fig. 1 Highlighted applications of carbenium ions. (a) Rhodamine dyes for bioimaging applications (R = alkyl), (b) acridiniums as photooxidants in photoredox catalysis, and (c) stabilized carbenium ions as electrolytes in organic redox flow batteries. (d) General structures and pK_{R+} values for *p*-functionalized and *o*-fused stable carbenium ions (R = alkyl). The combination of these two strategies is explored for the TriAzaTriangulenium (TATA$^+$) scaffold to synthesize highly stabilized carbenium ions with the highest recorded pK_{R+} values in literature. Anions are omitted for clarity.

a consequence of the electron-donating bridging heteroatoms, which planarize and rigidify the structure, leading to exceptional stabilities and bright fluorescence. The trianguleniums are named according to the identity of the bridging heteroatoms, as follows:

TriOxaTriangulenium (TOTA$^+$), AzaDioxaTriangulenium (ADOTA$^+$), DiAzaOxaTriangulenium (DAOTA$^+$), and TriAzaTriangulenium (TATA$^+$).[1] High chemical stability and tunable optical and redox properties have paved the way for their applications as fluorescent dyes with a wide array of implementations, including pH probes and sensors,[41–45] chiral emitters,[46–49] fluorescence lifetime probes for proton transfer,[50,51] and G-quadruplex DNA.[52–56] In recent years, the applications have expanded into photoredox catalysis,[57–64] CO_2 reduction,[65–67] hydrogen production,[68,69] and electrolytes in organic redox flow batteries.[27–30,70] The planar cationic nature of trianguleniums has been used to create ionic assemblies for applications as solid-state optical materials.[71–75] We have previously combined *p*-functionalization with *o*-fusion to synthesize tris(dialkylAmino)-TOTA$^+$ (A-TOTA$^+$) and tris(dialkylAmino)-ADOTA$^+$ (A-ADOTA$^+$), leading to more highly stabilized carbenium ions.[38,40] Among the triangulenium salts, TATA$^+$ and A-ADOTA$^+$ are the most stable carbenium ions reported to date, with pK_{R+} values of 23 and 25, respectively.[1,40] Further stabilizing the triangulenium ions is critical for expanding their use as catalysts under highly basic and/or nucleophilic conditions, extending the redox window for energy storage applications, and lowering the reduction potential to increase the potency as photoreductants.

To create further stabilized triangulenium salts, we envisioned the extension of the TATA$^+$ scaffold with electron-donating groups in the *p*-positions. However, it turns out that this cannot be realized through conventional nucleophilic aromatic substitution (S_NAr) reactions on the tris(2,4,6-trimethoxyphenyl)carbenium precursor as realized for A-ADOTA$^+$ and all other trianguleniums.[40] The very successful S_NAr synthesis strategy for trianguleniums is driven by the electron deficiency of the cationic substrates. However, as the cation stability increases the electrophilic reactivity decreases, with substitutions becoming fully suppressed for A-ADOTA$^+$ (pK_{R+} = 25), setting a limit for this synthetic strategy. Therefore, we explored different avenues, inspired by recent literature on the Ir-catalyzed borylation of triangulenium species.[76–78] This led to the successful synthesis of *p*-substituted TATA$^+$ derivatives tris(dialkylAmino)-TriAzaTriangulenium (A-TATA$^+$) and tris(Methoxy)-TriAzaTriangulenium (MeO-TATA$^+$).

Results and discussion

Synthesis and solid-state structure analysis

Starting from *N*-octyl-TATA$^+$, the *p*-borylated species (**3**) was obtained in excellent yield through Ir-catalyzed borylation with bis(1,5-cyclooctadiene)di-μ-methoxydiiridium(I) ([Ir(cod)OMe]$_2$) and 3,4,7,8-tetramethyl-1,10-phenanthroline (Me_4phen) as the catalyst system (Scheme 1a).[76] From here, several attempts were made at Chan–Lam couplings with pyrrolidine to obtain the A-TATA$^+$ framework directly from **3**. However, they were not successful due to competing oxidation and protodeborylation reactions which led to complex mixtures of products. Therefore, other strategies were explored, starting with oxidation of the boronic esters and ion exchange with KPF_6 to yield the poorly soluble tris(hydroxy)-TATA$^+$ (**4**). From here, alkylation with

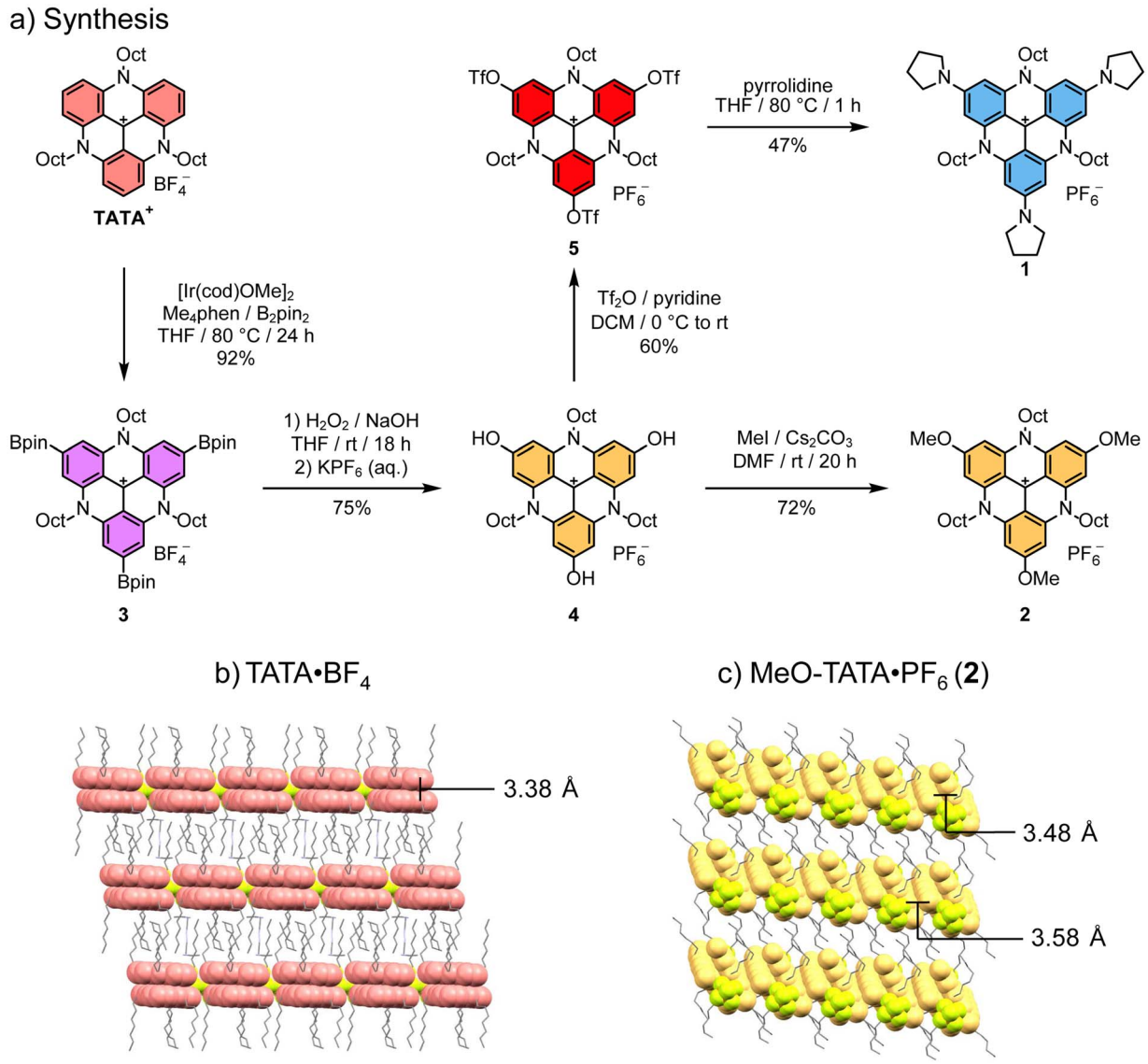

Scheme 1 (a) Synthesis of the *p*-substituted triangulenium dyes A-TATA$^+$ (**1**) and MeO-TATA$^+$ (**2**). (b) Crystal packing of TATA·BF_4 (redrawn from CIF file: CCDC 148692).[1] (c) Crystal packing of MeO-TATA·PF_6.

methyl iodide and Cs_2CO_3 as the base yielded tris(methoxy)-TATA$^+$ (MeO-TATA$^+$, **2**). Triflation of tris(hydroxy)-TATA$^+$ **4** using trifluoromethanesulfonic anhydride (Tf_2O) and pyridine as the base was achieved to afford the reactive tris(TfO)-TATA$^+$ (**5**). A threefold S_NAr reaction with pyrrolidine in anhydrous THF was possible with careful exclusion of water to form tris(pyrrolidine)-TATA$^+$ (A-TATA$^+$, **1**). The compound was purified by column chromatography to remove the undesired S–O scission hydroxy-byproducts formed during the reaction. The crystal structure of MeO-TATA$^+$ (**2**) was determined by electron diffraction (SI section 1.9), on microcrystals obtained by layering a $CHCl_3$ solution with i-PrOH, followed by slow diffusion at −25 °C. The experimental solid-state structure of MeO-TATA·PF_6 confirms the planarity of the triangulenium core (Fig. S56). In the crystal structure, MeO-TATA$^+$ (**2**) packs in slipped stacks of dimers with two distinct interplanar distances of 3.48 Å and 3.58 Å (Scheme 1c and Fig. S56). Layers of parallel stacks are separated by the kinked octyl chains that form hydrophobic layers between the layers of stacked TATA$^+$ cores. This crystal packing is in contrast to the parent TATA$^+$, which persistently forms 2D layers of TATA$^+$-dimers with inter planar distances of 3.38 Å separated by layers of straight interdigitated alkyl chains (Scheme 1b).[1,79,80] We tentatively assign the difference in solid-state packing to the increased footprint of the planar TATA$^+$ core due to the added methoxy-groups, which reduce the relative volume of the alkyl chains inducing their bending and the tilting of the TATA$^+$ dimers in the ionic layers.

Carbocation stability studies

With the *p*-substituted TATA$^+$ dyes **1** and **2** in hand, we set out to characterize their cation stabilities. In previous work, a solvent system of DMSO and H_2O with tetramethylammonium

hydroxide as the hydroxide source was used to determine quantitative pK_{R+} values for stable carbenium ions.[1,38,40,81–84] This system is, however, not applicable for pK_{R+} values above 25 due to competing irreversible reactions at the carbenium ions.[40] Therefore, we first sought to probe the chemical stability of the *p*-substituted A-TATA$^+$ using a qualitative method. The dyes TATA$^+$ and A-TATA$^+$ were dissolved in MeOH in a cuvette, where an excess of the strong hydride donor $NaBH_4$ was subsequently added. Absorption spectra as a function of time after addition of $NaBH_4$ are shown in Fig. 2 aiming to follow the addition of hydride to the cation in solution ($C^+ + H^- \rightarrow C\text{–}H$). TATA$^+$ is slowly reduced to the colorless TATA-H upon reaction with $NaBH_4$, as indicated by the decrease in absorption at 525 nm, while A-TATA$^+$ is not affected by the addition of $NaBH_4$, clearly demonstrating the enhanced chemical stability of A-TATA$^+$, suggesting a significantly higher pK_{R+} than TATA$^+$ ($pK_{R+} = 23.4$). This enhanced cation stability is also expected to be reflected in a more negative reduction potential.

We conducted cyclic voltammetry and differential pulse voltammetry experiments in MeCN with tetrabutylammonium hexafluorophosphate ($TBAPF_6$, $c = 0.1$ M) as the electrolyte to determine the E_{red} of the trianguleniums presented herein, varying the scan rate from 0.1 to 1 V s^{-1} (SI section 1.3). The normalized voltammograms at scan-rates where reduction is quasi-reversible are shown in Fig. 3. The voltammograms show clear shifts in the reduction potentials due to the addition of electron-donating groups in the *p*-positions of TATA$^+$, with E_{red} shifted by 300 mV for MeO-TATA$^+$ (**2**) and by as much as 700 mV for A-TATA$^+$ (**1**). This is a clear demonstration of the large cation-stabilizing effect of the *p*-donor groups and highlights potential applications of A-TATA$^+$ as a stronger electron donor for photoredox catalysis.[66–69]

The one-electron reduction potential and the pK_{R+} value are both measures of carbenium ion stabilities, and work by Okamoto *et al.* suggests a correlation between the two parameters for structurally related tropyllium ions.[85] The reduction potential can be considered to reflect mainly two terms: the electron affinity governed by the molecular structure, and the change in solvation energy between the cation and the neutral radical.[86] The pK_{R+} value has an additional term, which depends on the strain energy difference between the cation and the carbinol product.[85,86] Within a family of compounds, like the trianguleniums, the solvation and strain energies are expected to be similar due to the comparable structure of the compounds, so E_{red} and the pK_{R+} values should be proportional. To probe the proportionality, the pK_{R+} and E_{red} values for several families of carbenium ions were plotted (SI section 1.4). These relationships are linear, though each with different slopes (Fig. S21), suggesting E_{red} and pK_{R+} values are indeed proportional within families of carbenium ions. To explore the correlation between reduction potentials and pK_{R+} values for the trianguleniums, reported pK_{R+} values were plotted as a function of E_{red}

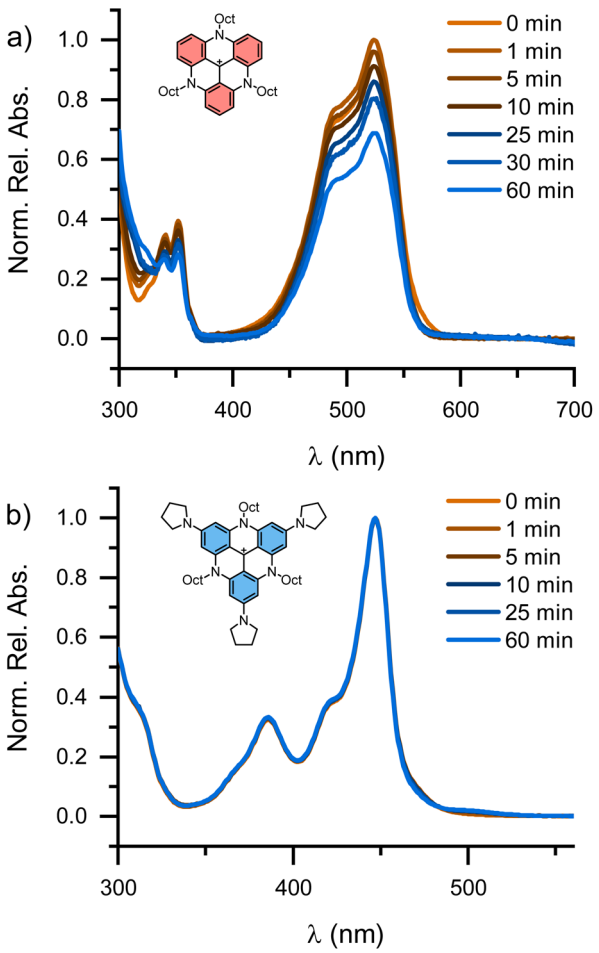

Fig. 2 Absorption spectra of the triangulenium dyes TATA$^+$ (a) and A-TATA$^+$ (b) in MeOH after addition of solid $NaBH_4$ at consecutive time points up to 60 min. Anions are omitted for clarity.

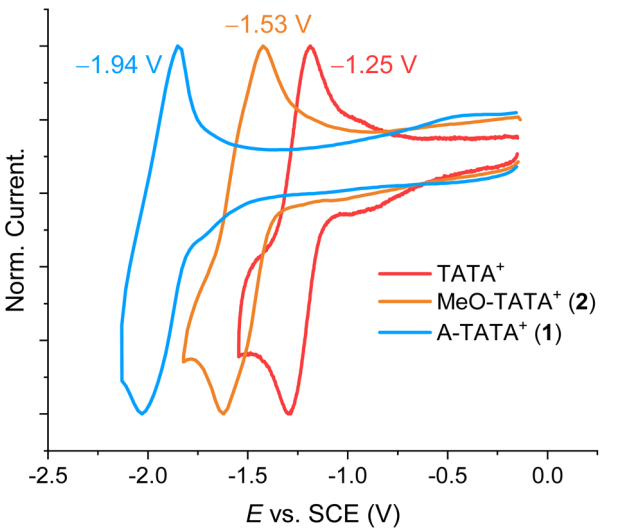

Fig. 3 Normalized cyclic voltammograms of the triangulenium dyes TATA$^+$ (red, $\nu = 0.1$ V s^{-1}), MeO-TATA$^+$ (**2**) (orange, $\nu = 1$ V s^{-1}), and A-TATA$^+$ (**1**) (blue, $\nu = 1$ V s^{-1}) at quasi-reversible scan-rates. Recorded in MeCN at rt with $TBAPF_6$ ($c = 0.1$ M) as the supporting electrolyte. Analyte concentrations are 0.5 mM. WE, glassy carbon $\varnothing = 2$ mm; RE, Ag/Ag$^+$; CE, Pt wire. All potentials are recorded *vs.* Fc/Fc$^+$ and converted to SCE by addition of 380 mV.[2]

determined by cyclic voltammetry in MeCN with $TBAPF_6$ (0.1 M) as the supporting electrolyte (electrochemical data is reported in SI section 1.3).[1,37,38,40] The proportional nature between pK_{R+} and E_{red} is clearly illustrated in Fig. 4b, showcasing a near-perfect linear relationship between the two parameters. The linear relationship for the trianguleniums allows us to estimate the pK_{R+} values for the *p*-substituted $TATA^+$ dyes MeO-$TATA^+$ (**2**) and A-$TATA^+$ (**1**) to be 26 and 32, respectively. The obtained pK_{R+} values are far higher than any previously reported pK_{R+} values and clearly outside the range that can be measured experimentally with previously developed methods. To consolidate these findings and further investigate the cation stabilities of the trianguleniums, we approached the problem from a computational standpoint. The Gibbs free energy for the carbinol-forming reaction ($C^+ + OH^- \rightleftharpoons COH$) was determined at DFT level of theory (SI section 1.6, Table S7). The pK_{R+} values for the trianguleniums were plotted as a function of the computed ΔG values (Fig. 4c). These parameters are also linearly correlated, suggesting the estimated pK_{R+} values for A-$TATA^+$ and MeO-$TATA^+$ based on E_{red} are valid. These stability constants are the highest for any carbenium ion reported in the literature to our knowledge, making A-$TATA^+$ the most stable carbenium ion reported to date. With this extension of the triangulenium family we can start to analyze and quantify the effects of *p*-substituents and bridging heteroatoms on the cation stability and reduction potentials (data collected in Table S4).[1,37,38,40] Comparing $TATA^+$ ($pK_{R+} = 23$) to $TOTA^+$ ($pK_{R+} = 9$) the effect of N *vs.* O bridging is clear, increasing the stability by 14 units on the pK_{R+} scale. This effect is somewhat smaller for *p*-substitution as demonstrated by $TOTA^+$ ($pK_{R+} = 9$) *vs.* A-$TOTA^+$ ($pK_{R+} = 19$), where adding electron-donating amines increases the stability by 10 units on the pK_{R+} scale. Adding three *p*-amino groups to $TATA^+$, giving A-$TATA^+$ ($pK_{R+} = 32$), raises the pK_{R+} by another 9 pK_{R+} units indicating that the effects are additive and largely independent of the triangulenium core. To further explore the relationship between cation stability and electronic structure of the trianguleniums, the charge distribution on the central carbon atom was calculated using the DDEC6 charge-partitioning scheme (Table S8).[87–89] DDEC6 is a modern and efficient net atomic charge (NAC) scheme that avoids inconsistencies between symmetry-related atoms and is tailored to provide an accurate description of 'buried' atoms. Plotting the atomic charge as a function of the pK_{R+} values for the trianguleniums reveals two linearly correlated populations (Fig. 4d), one with the strictly *o*-fused trianguleniums and one with the *p*-amino functionalized. The single case of *p*-methoxy triangulenium (**2**) falls in between. These results suggest that the impact of *p*-functionalization of the triangulenium system on E_{red} and pK_{R+} goes beyond simple charge delocalization. For instance, A-$TATA^+$ and $TATA^+$ have similar partial charges (+0.099 and +0.105, respectively) on the central carbon despite pK_{R+} values differing by 9 units. In fact, the main effect of *p*-amino substituents consists in raising both HOMO and LUMO energies, to different extents but in a correlated way, with respect to the unsubstituted analogs (Fig. 5). According to DFT calculations, HOMO and LUMO destabilization amounts to 0.57 eV and 0.91 eV, respectively, going from $TATA^+$ to A-$TATA^+$, consistent with the respective increase in pK_{R+} and $|E_{red}|$ values.

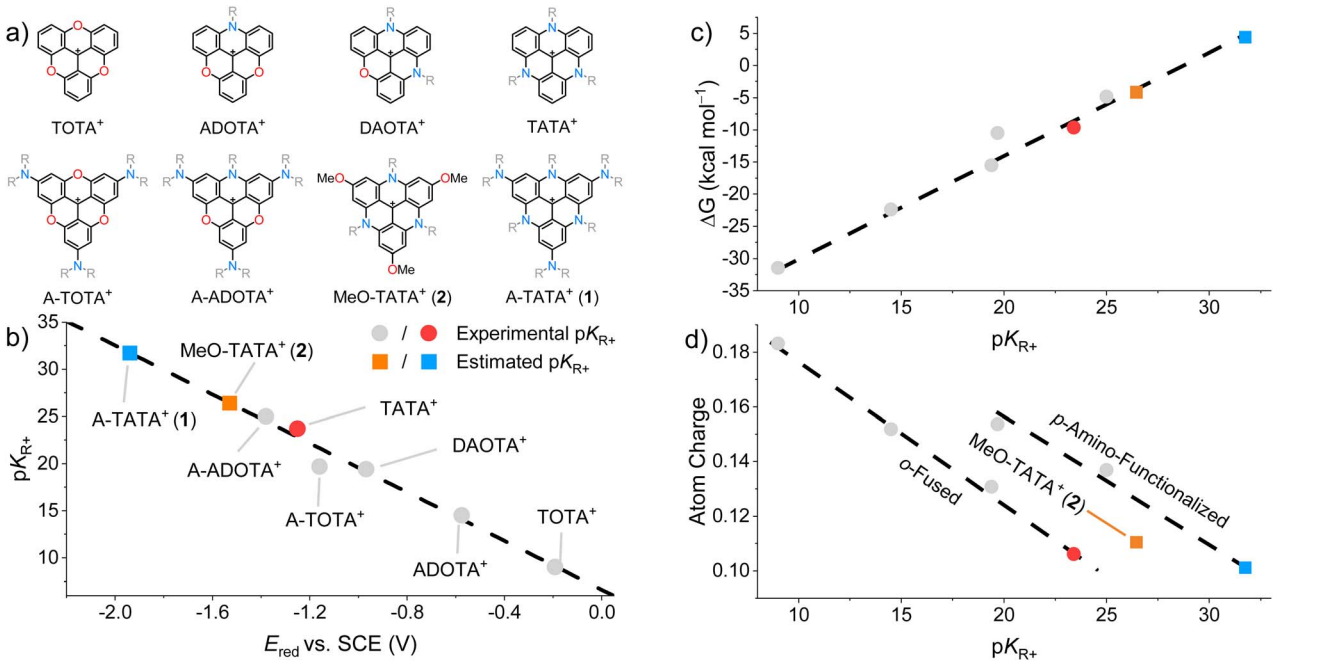

Fig. 4 (a) General structures of the trianguleniums with R = alkyl. (b) Carbocation stability (pK_{R+}) as a function of reduction potential (E_{red}) for the trianguleniums. (c) Correlation between DFT-calculated ΔG values for the reaction $C^+ + OH^- \rightleftharpoons COH$ and pK_{R+}. (d) Correlation between DFT-calculated central carbon charge (DDEC6 scheme) and pK_{R+}. The ● data points are experimentally determined pK_{R+} values, while the ■ data points are estimated pK_{R+} values from the linear relationship between pK_{R+} and E_{red} represented by the dashed line in (b). Anions are omitted for clarity.

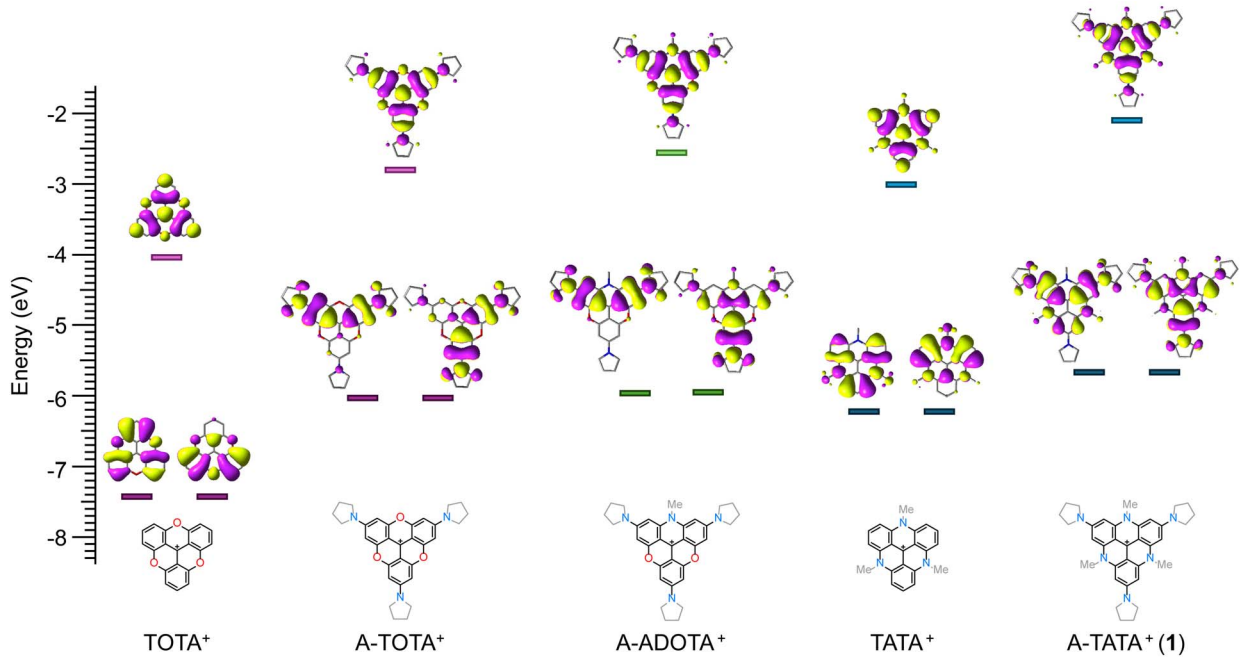

Fig. 5 HOMO and LUMO Kohn–Sham orbitals and relative energies (eV) computed by DFT at B3LYP-D3BJ/6-311+G(2d,p) level of theory, including a continuum solvent model (IEF-PCM) for CH_2Cl_2, for TOTA$^+$, A-TOTA$^+$, and truncated NMe analogs of A-ADOTA$^+$, TATA$^+$ and A-TATA$^+$ (**1**).

Optical properties

The triangulenium family of carbenium ions is characterized by their exceptional cation stability combined with very favorable optical properties, enabling their applications as fluorescent dyes and probes, as well as photoredox catalysts.[62] Triangulenium without *p*-donor groups display unique photophysical properties with long fluorescence lifetimes ($\tau > 20$ ns in the case of ADOTA$^+$ and DAOTA$^+$) which have been key to many fluorescence assays and imaging applications.[52,54–56,90–96] The introduction of *p*-amino groups in A-TOTA$^+$ and A-ADOTA$^+$, on the other hand, leads to high molar absorption coefficients and short lifetimes ($\tau \approx 4$ ns) akin to rhodamines, and these dyes are used as chemically stable, bright fluorescent labels.[97] Therefore, we investigated the photophysical properties of the new triangulenium dyes MeO-TATA$^+$ (**2**) and A-TATA$^+$ (**1**) in CH_2Cl_2, and compared them to the parent TATA$^+$ fluorophore (SI section 1.5). The normalized absorption spectra and the emission spectra scaled to the fluorescence quantum yields are shown in Fig. 6. Detailed emission and excitation spectra are provided in SI section 1.5.1. The absorption coefficients,

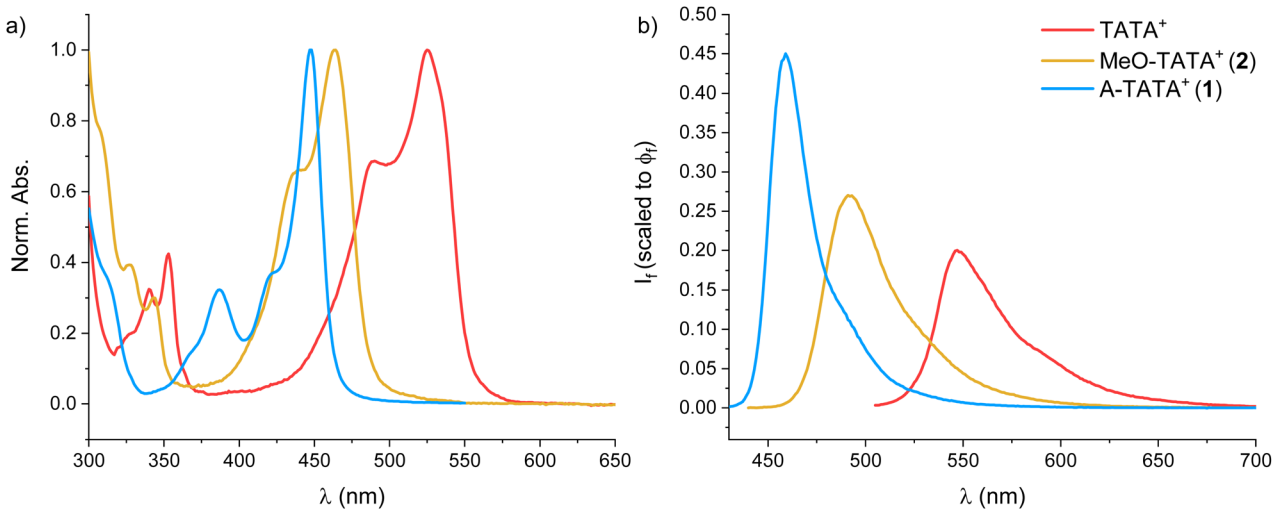

Fig. 6 (a) Normalized absorption spectra of the TATA$^+$ dyes in CH_2Cl_2, (b) Emission spectra scaled to the fluorescence quantum yield for the TATA$^+$ dyes in CH_2Cl_2.

Table 1 Optical properties for the trianguleniums in CH_2Cl_2. Molar absorption coefficient (ε), fluorescence quantum yield (Φ_f), average fluorescence lifetime ($\tau_{avg.}$) in CH_2Cl_2, along with the calculated rate constants for radiative (k_f) and non-radiative (k_{nr}) processes

	ε [M^{-1} cm^{-1}]	$\lambda_{abs}/\lambda_{emi}$ [nm]	τ_{avg} [ns]	ϕ_f [%][a]	k_f [10^7 s^{-1}]	k_{nr} [10^7 s^{-1}]
$TATA^+$	19 000	525/548	6.6	21	3.2	12
MeO-$TATA^+$ (**2**)	26 000	463/485	4.6	28	6.0	16
A-$TATA^+$ (**1**)	84 000	447/460	2.7	45	17	20
A-$TOTA^+$	132 000[b]	472/495	3.0	93	31	2
A-$ADOTA^+$	120 000[c]	458/479	2.7	73	27	10

[a] Quantum yields are determined relative to coumarin-153 in EtOH ($\phi_f = 54\%$).[98] For $TATA^+$ the quantum yield was determined relative to Rho-6G in EtOH ($\phi_f = 94\%$).[99] [b] Data from Laursen *et al.*[100] [c] Data from Laursen and Sørensen.[40]

fluorescence lifetimes, fluorescence quantum yields, and associated rate constants are given in Table 1, with additional data provided in SI sections 1.5.2 and 1.5.3.

From the absorption spectra, we observe a clear blue-shift in the absorption maxima as stronger electron donors are introduced in the *p*-positions, with A-$TATA^+$ having an absorption maximum at 447 nm. The shift in absorption maxima is well reproduced by TD-DFT calculations (CAM-B3LYP/def2-TZVP/PCM level, Table S9 and Fig. S41). The same trend is observed in the emission spectra, drastically blue-shifting the fluorescence with increasing electron donor strength. Interestingly, the fluorescence quantum yield increases two-fold from $TATA^+$ to A-$TATA^+$ (from 20% to 45%). This is accompanied by a decrease in fluorescence lifetime from 6.6 to 2.7 ns for A-$TATA^+$, reflecting a fivefold increase in the radiative rate constant (k_f) from 3.0×10^7 to 16×10^7 s^{-1}. The non-radiative rate constant (k_{nr}) increases marginally from 12×10^7 to 20×10^7 s^{-1}, suggesting that *p*-functionalization also introduces additional non-radiative decay pathways.

All told, the introduction of electron donating groups in the *p*-positions makes the $TATA^+$ scaffold a more efficient fluorophore with significantly blue-shifted optical properties. Excitation at 447 nm with a high molar absorption coefficient, good ϕ_f, and a small Stokes shift is rare for carbenium ions, and suggests that A-$TATA^+$ derivatives could find applications in imaging and bioassays, especially when modified for water solubility and bioconjugation, or in other applications where cationic chromophores are needed.[72,101,102] This spectral range is usually reserved for coumarins,[5,103] substituted pyrenes,[104–106] and multiple-resonant emitters for OLEDs.[107] The changes in the optical properties can be rationalized using Dewar's perturbation molecular orbital theory approach, which has proven to be a good model for trianguleniums and related systems.[108] The pair of HOMO orbitals of $TATA^+$ has a node in the para positions (Fig. 5). Thus, introduction of electron-donating groups will predominantly destabilize the LUMO, and to a lesser extent the HOMO, leading to a blue-shift in the optical properties, namely S_0–S_1 and S_1–S_0 transitions, which are mainly associated with HOMO–LUMO single (de-)excitations. This explanation agrees with the redox properties, where A-$TATA^+$'s E_{red} is significantly more negative ($\Delta E = -0.7$ V, Fig. 3) compared to $TATA^+$, while the oxidation potential is less affected ($\Delta E = -0.33$ V, Table S1). These values agree with the shift in absorption maxima of 0.4 eV.

Conclusions

In summary, we have presented herein the synthesis of $TATA^+$ derivatives with electron-donating groups (methoxy and amino) in the *p*-positions. These new trianguleniums MeO-$TATA^+$ (**2**) and A-$TATA^+$ (**1**) are among the most stable carbenium ions, with A-$TATA^+$ having the highest cation stability ever reported with a pK_{R+} value of 32. The stability is accompanied by an exceptionally low $E_{red} = -1.94$ V *vs.* SCE, suggesting that A-$TATA^+$ has potential applications as a photoreducant in photoredox catalysis. The new trianguleniums show promising dye properties with intense absorption in the blue region of the visible spectrum at 447 nm ($\varepsilon = 84000$ M^{-1} cm^{-1}) and efficient fluorescence at 460 nm ($\phi_f = 45\%$) in CH_2Cl_2 solution.

Author contributions

M. H. N contributed with writing – original draft & review & editing, conceptualization, investigation, formal analysis, data curation, and methodology. G. P. contributed with writing – review & editing, investigation, formal analysis, data curation, and methodology. A. L. contributed with writing – review & editing, investigation, data curation, and formal analysis. B. W. L. contributed with writing – review & editing, conceptualization, funding acquisition, methodology, supervision, and project administration.

Conflicts of interest

There are no conflicts to declare.

Data availability

CCDC 2524713 MeO-$TATA^+$ (**2**) contains the supplementary crystallographic data for this paper.[123]

The supporting data has been provided as part of the supplementary information (SI). The authors have cited additional references within the SI.[109–122] Supplementary information: experimental details and synthetic procedures, NMR spectra, HRMS spectra, detailed absorption and emission spectra of new compounds, additional computational details, electron difraction methods and crystal structure data. See DOI: https://doi.org/10.1039/d6sc01535b.

Acknowledgements

The Novo Nordisk Foundation is acknowledged for financially supporting this work (grant NNF20OC0062176). Electron diffraction experiments are supported by Novo Nordisk Foundation Research Infrastructure (grant NNF220C0074439). The Novo Nordisk Foundation is also acknowledged for NMR facility (grant NNF21OC0067315). G.P. acknowledges the support and computational resources provided by computing@unipi, a Computing Service provided by the University of Pisa.

Notes and references

1 B. W. Laursen and F. C. Krebs, *Chem. – Eur. J.*, 2001, **7**, 1773–1783.
2 V. V. Pavlishchuk and A. W. Addison, *Inorg. Chim. Acta*, 2000, **298**, 97–102.
3 D. F. Duxbury, *Chem. Rev.*, 1993, **93**, 381–433.
4 K. H. Drexhage, in *Dye Lasers*, ed. F. P. Schäfer, Springer Berlin Heidelberg, Berlin, Heidelberg, 1973, pp. 144–193.
5 L. D. Lavis and R. T. Raines, *ACS Chem. Biol.*, 2008, **3**, 142–155.
6 L. D. Lavis, *Annu. Rev. Biochem.*, 2017, **86**, 825–843.
7 J. Griffiths, *Colour and Constitution of Organic Molecules*, Academic Press, 1976.
8 T. Terai and T. Nagano, *Pflugers Arch.*, 2013, **465**, 347–359.
9 H. Mustroph, *Phys. Sci. Rev.*, 2020, **5**, 20190145.
10 M. J. Schnermann and L. D. Lavis, *Curr. Opin. Chem. Biol.*, 2023, **75**, 102335.
11 J. Arden-Jacob, J. Frantzeskos, N. U. Kemnitzer, A. Zilles and K. H. Drexhage, *Spectrochim. Acta, Part A*, 2001, **57**, 2271–2283.
12 K. Kolmakov, V. N. Belov, C. A. Wurm, B. Harke, M. Leutenegger, C. Eggeling and S. W. Hell, *Eur. J. Org Chem.*, 2010, **2010**, 3593–3610.
13 T. Egawa, Y. Koide, K. Hanaoka, T. Komatsu, T. Terai and T. Nagano, *Chem. Commun.*, 2011, **47**, 4162–4164.
14 Y. Koide, Y. Urano, K. Hanaoka, T. Terai and T. Nagano, *ACS Chem. Biol.*, 2011, **6**, 600–608.
15 J. B. Grimm, A. J. Sung, W. R. Legant, P. Hulamm, S. M. Matlosz, E. Betzig and L. D. Lavis, *ACS Chem. Biol.*, 2013, **8**, 1303–1310.
16 J. B. Grimm, T. A. Brown, A. N. Tkachuk and L. D. Lavis, *ACS Cent. Sci.*, 2017, **3**, 975–985.
17 H. Kotani, K. Ohkubo and S. Fukuzumi, *J. Am. Chem. Soc.*, 2004, **126**, 15999–16006.
18 C. Nicolas, C. Herse and J. Lacour, *Tetrahedron Lett.*, 2005, **46**, 4605–4608.
19 K. Ohkubo, K. Mizushima, R. Iwata and S. Fukuzumi, *Chem. Sci.*, 2011, **2**, 715.
20 D. S. Hamilton and D. A. Nicewicz, *J. Am. Chem. Soc.*, 2012, **134**, 18577–18580.
21 N. A. Romero, K. A. Margrey, N. E. Tay and D. A. Nicewicz, *Science*, 2015, **349**, 1326–1330.
22 A. Joshi-Pangu, F. Lévesque, H. G. Roth, S. F. Oliver, L.-C. Campeau, D. Nicewicz and D. A. Dirocco, *J. Org. Chem.*, 2016, **81**, 7244–7249.
23 C. Fischer, C. Kerzig, B. Zilate, O. S. Wenger and C. Sparr, *ACS Catal.*, 2020, **10**, 210–215.
24 V. Hutskalova and C. Sparr, *Org. Lett.*, 2021, **23**, 5143–5147.
25 J. D. Jensen, N. Bisballe, L. Kacenauskaite, M. S. Thomsen, J. Chen, O. Hammerich and B. W. Laursen, *J. Org. Chem.*, 2021, **86**, 17002–17010.
26 M. H. Nowack, M. B. Johansen, S. Sams, A. E. Hillers-Bendtsen, K. V. Mikkelsen and B. W. Laursen, *Chem. – Eur. J.*, 2025, **31**, e202403451.
27 J. Moutet, J. M. Veleta and T. L. Gianetti, *ACS Appl. Energy Mater.*, 2021, **4**, 9–14.
28 J. Moutet, D. Mills, M. M. Hossain and T. L. Gianetti, *Mater. Adv.*, 2022, **3**, 216–223.
29 J. Moutet, M. H. Nowack, D. Mills, D. L. Lozier, B. W. Laursen and T. L. Gianetti, *Mater. Adv.*, 2023, **4**, 4598–4606.
30 J. Moutet, T. H. El-Assaad, R. Kaur, D. D. Mills and T. L. Gianetti, *Energy Mater.*, 2024, **4**, 400024.
31 J. Bosson, J. Gouin and J. Lacour, *Chem. Soc. Rev.*, 2014, **43**, 2824–2840.
32 V. Dujols, F. Ford and A. W. Czarnik, *J. Am. Chem. Soc.*, 1997, **119**, 7386–7387.
33 L. D. Lavis, T.-Y. Chao and R. T. Raines, *ACS Chem. Biol.*, 2006, **1**, 252–260.
34 X. Chen, T. Pradhan, F. Wang, J. S. Kim and J. Yoon, *Chem. Rev.*, 2012, **112**, 1910–1956.
35 A. N. Butkevich, G. Y. Mitronova, S. C. Sidenstein, J. L. Klocke, D. Kamin, D. N. H. Meineke, E. D'Este, P.-T. Kraemer, J. G. Danzl, V. N. Belov and S. W. Hell, *Angew. Chem., Int. Ed.*, 2016, **55**, 3290–3294.
36 V. Gold and B. W. V. Hawes, *J. Chem. Soc.*, 1951, 2102–2111.
37 J. C. Martin and R. G. Smith, *J. Am. Chem. Soc.*, 1964, **86**, 2252–2256.
38 B. W. Laursen, F. C. Krebs, M. F. Nielsen, K. Bechgaard, J. B. Christensen and N. Harrit, *J. Am. Chem. Soc.*, 1998, **120**, 12255–12263.
39 C. Nicolas and J. Lacour, *Org. Lett.*, 2006, **8**, 4343–4346.
40 B. W. Laursen and T. J. Sørensen, *J. Org. Chem.*, 2009, **74**, 3183–3185.
41 A. Wallabregue, D. Moreau, P. Sherin, P. Moneva Lorente, Z. Jarolímová, E. Bakker, E. Vauthey, J. Gruenberg and J. Lacour, *J. Am. Chem. Soc.*, 2016, **138**, 1752–1755.
42 T. J. Sørensen, M. Rosenberg, C. G. Frankær and B. W. Laursen, *Adv. Mater. Technol.*, 2018, **4**, 1800561.
43 M. Rosenberg, A. K. R. Junker, T. J. Sørensen and B. W. Laursen, *ChemPhotoChem*, 2019, **3**, 233–242.
44 C. G. Frankær, M. Rosenberg, M. Santella, K. J. Hussain, B. W. Laursen and T. J. Sørensen, *ACS Sens.*, 2019, **4**, 764–773.
45 I. Dalfen, R. I. Dmitriev, G. Holst, I. Klimant and S. M. Borisov, *Anal. Chem.*, 2019, **91**, 808–816.
46 C. Herse, D. Bas, F. C. Krebs, T. Bürgi, J. Weber, T. Wesolowski, B. W. Laursen and J. Lacour, *Angew. Chem., Int. Ed.*, 2003, **42**, 3162–3166.
47 O. Kel, P. Sherin, N. Mehanna, B. Laleu, J. Lacour and E. Vauthey, *Photochem. Photobiol. Sci.*, 2012, **11**, 623–631.

48 S. Pascal, C. Besnard, F. Zinna, L. Di Bari, B. Le Guennic, D. Jacquemin and J. Lacour, *Org. Biomol. Chem.*, 2016, **14**, 4590–4594.
49 B. Fabri, D. F. De Rosa, D. J. Black, R. Mucci, A. Krimovs, R. Pal and J. Lacour, *Chem. – Eur. J.*, 2025, **31**, e202501212.
50 R. K. Jakobsen, S. G. Stenspil, J. Chen and B. W. Laursen, *Chem. Sci.*, 2025, **16**, 7450–7458.
51 M. H. Nowack and B. W. Laursen, *Chemphotochem*, 2025, **9**, 2500183.
52 A. Shivalingam, M. A. Izquierdo, A. L. Marois, A. Vyšniauskas, K. Suhling, M. K. Kuimova and R. Vilar, *Nat. Commun.*, 2015, **6**, 8178.
53 A. Kotar, B. Wang, A. Shivalingam, J. Gonzalez-Garcia, R. Vilar and J. Plavec, *Angew. Chem., Int. Ed.*, 2016, **55**, 12508–12511.
54 A. Shivalingam, A. Vyšniauskas, T. Albrecht, A. J. P. White, M. K. Kuimova and R. Vilar, *Chem. – Eur. J.*, 2016, **22**, 4129–4139.
55 B. W. Lewis, N. Bisballe, M. Santella, P. A. Summers, J. B. Vannier, M. K. Kuimova, B. W. Laursen and R. Vilar, *Chem. – Eur. J.*, 2021, **27**, 2523–2536.
56 P. A. Summers, B. W. Lewis, J. Gonzalez-Garcia, R. M. Porreca, A. H. M. Lim, P. Cadinu, N. Martin-Pintado, D. J. Mann, J. B. Edel, J. B. Vannier, M. K. Kuimova and R. Vilar, *Nat. Commun.*, 2021, **12**, 162.
57 L. Mei, J. M. Veleta and T. L. Gianetti, *J. Am. Chem. Soc.*, 2020, **142**, 12056–12061.
58 S. M. Stull, L. Mei and T. L. Gianetti, *Synlett*, 2021, **33**, 1194–1198.
59 L. Mei, J. Moutet, S. M. Stull and T. L. Gianetti, *J. Org. Chem.*, 2021, **86**, 10640–10653.
60 M. M. Hossain, A. C. Shaikh, J. Moutet and T. L. Gianetti, *Nat. Synth.*, 2022, **1**, 147–157.
61 F. Calogero, G. Magagnano, S. Potenti, F. Pasca, A. Fermi, A. Gualandi, P. Ceroni, G. Bergamini and P. G. Cozzi, *Chem. Sci.*, 2022, **13**, 5973–5981.
62 M. H. Nowack, J. Moutet, B. W. Laursen and T. L. Gianetti, *Synlett*, 2024, **35**, 307–312.
63 M. M. Hossain, A. C. Shaikh, R. Kaur and T. L. Gianetti, *J. Am. Chem. Soc.*, 2024, **146**, 7922–7930.
64 K. A. Ryu, T. Reyes-Robles, T. P. Wyche, T. J. Bechtel, J. M. Bertoch, J. Zhuang, C. May, C. Scandore, N. Dephoure, S. Wilhelm, I. Quasem, A. Yau, S. Ingale, A. Szendrey, M. Duich, R. C. Oslund and O. O. Fadeyi, *ACS Catal.*, 2024, **14**, 3482–3491.
65 P.-Y. Ho, S.-C. Cheng, F. Yu, Y.-Y. Yeung, W.-X. Ni, C.-C. Ko, C.-F. Leung, T.-C. Lau and M. Robert, *ACS Catal.*, 2023, **13**, 5979–5985.
66 S. Hao, K.-K. Chen, P. Liang, Q. Huang, L. Zhou, Y. Wei and Z. Wei, *Nat. Commun.*, 2025, **16**, 6167.
67 S. Hao, Z. Wang, K. K. Chen, Y. Wei, L. Zhou and Z. Wei, *ChemCatChem*, 2025, **17**, e00733.
68 R. Gueret, L. Poulard, M. Oshinowo, J. Chauvin, M. Dahmane, G. Dupeyre, P. P. Lainé, J. Fortage and M.-N. Collomb, *ACS Catal.*, 2018, **8**, 3792–3802.
69 S. Lyu, D. H. Cruz Neto, J. Aguirre-Araque, L. Termeau, F. Camara, S. Cherraben, D. Martin, E. Brémond, T. Pino, M.-H. Ha-Thi, P. P. Lainé, M.-N. Collomb and J. Fortage, *Artif. Photosynth.*, 2025, **1**, 251–266.
70 J. Moutet, D. D. Mills, D. L. Lozier and T. L. Gianetti, *Batter. Supercaps*, 2024, **7**, e202300519.
71 Y. Haketa, S. Sasaki, N. Ohta, H. Masunaga, H. Ogawa, N. Mizuno, F. Araoka, H. Takezoe and H. Maeda, *Angew. Chem., Int. Ed.*, 2010, **49**, 10079–10083.
72 C. R. Benson, L. Kacenauskaite, K. L. VanDenburgh, W. Zhao, B. Qiao, T. Sadhukhan, M. Pink, J. Chen, S. Borgi, C.-H. Chen, B. J. Davis, Y. C. Simon, K. Raghavachari, B. W. Laursen and A. H. Flood, *Chem*, 2020, **6**, 1978–1997.
73 J. Chen, S. M. A. Fateminia, L. Kacenauskaite, N. Bærentsen, S. Grønfeldt Stenspil, J. Bredehoeft, K. L. Martinez, A. H. Flood and B. W. Laursen, *Angew. Chem., Int. Ed.*, 2021, **60**, 9450–9458.
74 Y. Haketa, K. Yamasumi and H. Maeda, *Chem. Soc. Rev.*, 2023, **52**, 7170–7196.
75 P. Deshmukh, S. Satapathy, E. Michail, A. H. Olsson, R. Bushati, R. K. Yadav, M. Khatoniar, J. Chen, G. John, B. W. Laursen, A. H. Flood, M. Y. Sfeir and V. M. Menon, *ACS Photonics*, 2024, **11**, 348–355.
76 H. Noguchi, T. Hirose, S. Yokoyama and K. Matsuda, *CrystEngComm*, 2016, **18**, 7377–7383.
77 L. Frédéric, B. Fabri, L. Guénée, F. Zinna, L. Di Bari and J. Lacour, *Chem. – Eur. J.*, 2022, **28**, e202201853.
78 B. Fabri, T. Funaioli, L. Frédéric, C. Elsner, E. Bordignon, F. Zinna, L. Di Bari, G. Pescitelli and J. Lacour, *J. Am. Chem. Soc.*, 2024, **146**, 8308–8319.
79 T. J. Sørensen, C. B. Hildebrandt, J. Elm, J. W. Andreasen, A. Ø. Madsen, F. Westerlund and B. W. Laursen, *J. Mater. Chem.*, 2012, **22**, 4797–4805.
80 T. J. Sørensen, C. B. Hildebrandt, M. Glyvradal and B. W. Laursen, *Dyes Pigm.*, 2013, **98**, 297–303.
81 T. J. Sørensen, M. F. Nielsen and B. W. Laursen, *ChemPlusChem*, 2014, **79**, 1030–1035.
82 D. Dolman and R. Stewart, *Can. J. Chem.*, 1967, **45**, 911–924.
83 S. Ito, S. Kikuchi, N. Morita and T. Asao, *J. Org. Chem.*, 1999, **64**, 5815–5821.
84 S. Ito, S. Kikuchi, N. Morita and T. Asao, *Bull. Chem. Soc. Jpn.*, 1999, **72**, 839–849.
85 K. Okamoto, K. i. Takeuchi, K. Komatsu, Y. Kubota, R. Ohara, M. Arima, K. Takahashi, Y. Waki and S. Shirai, *Tetrahedron*, 1983, **39**, 4011–4024.
86 M. R. Feldman and W. C. Flythe, *J. Org. Chem.*, 1978, **43**, 2596–2600.
87 N. G. Limas and T. A. Manz, *RSC Adv.*, 2016, **6**, 45727–45747.
88 T. A. Manz and N. G. Limas, *RSC Adv.*, 2016, **6**, 47771–47801.
89 N. G. Limas and T. A. Manz, *RSC Adv.*, 2018, **8**, 2678–2707.
90 T. J. Sørensen, E. Thyrhaug, M. Szabelski, R. Luchowski, I. Gryczynski, Z. Gryczynski and B. W. Laursen, *Methods Appl. Fluoresc.*, 2013, **1**, 25001.
91 B. P. Maliwal, R. Fudala, S. Raut, R. Kokate, T. J. Sørensen, B. W. Laursen, Z. Gryczynski and I. Gryczynski, *PLoS One*, 2013, **8**, e63043.
92 R. M. Rich, D. L. Stankowska, B. P. Maliwal, T. J. Sørensen, B. W. Laursen, R. R. Krishnamoorthy, Z. Gryczynski,

J. Borejdo, I. Gryczynski and R. Fudala, *Anal. Bioanal. Chem.*, 2013, **405**, 2065–2075.
93 R. Chib, M. Mummert, I. Bora, B. W. Laursen, S. Shah, R. Pendry, I. Gryczynski, J. Borejdo, Z. Gryczynski and R. Fudala, *Anal. Bioanal. Chem.*, 2016, **408**, 3811–3821.
94 A. Baibek, Z. Konieczna, M. Üçüncü, Z. S. Alghamdi, R. Sharma, M. H. Horrocks and M. Bradley, *Chem. Biomed. Imaging*, 2025, **3**, 45–50.
95 K. Kumar, T. H. Braunstein, P. Hernandez-Varas, M. B. Liisberg and B. W. Laursen, *J. Mater. Chem. B*, 2025, **13**, 13062–13074.
96 C. Viedma-Barba, E. M. Ortega-Naranjo, F. Movilla, A. Reinoso, M. Andrades-Amate, P. Peñalver, J. C. Morales, J. A. González-Vera, M. Gutiérrez-Rodríguez and A. Orte, *Sci. Rep.*, 2025, **16**, 1925.
97 Y. Zhang, J. Kæstel-Hansen, D. Teze, G. Huang, S. Schoffelen, M. Lisby, M. Zhang, N. S. Hatzakis and M. Meldal, *Angew. Chem., Int. Ed.*, 2025, **64**, e202504862.
98 K. Rurack and M. Spieles, *Anal. Chem.*, 2011, **83**, 1232–1242.
99 M. Fischer and J. Georges, *Chem. Phys. Lett.*, 1996, **260**, 115–118.
100 B. W. Laursen, J. Reynisson, K. V. Mikkelsen, K. Bechgaard and N. Harrit, *Photochem. Photobiol. Sci.*, 2005, **4**, 568–576.
101 L. Kacenauskaite, S. G. Stenspil, A. H. Olsson, A. H. Flood and B. W. Laursen, *J. Am. Chem. Soc.*, 2022, **144**, 19981–19989.
102 S. G. Stenspil, J. Chen, M. B. Liisberg, A. H. Flood and B. W. Laursen, *Chem. Sci.*, 2024, **15**, 5531–5538.
103 W.-C. Sun, K. R. Gee and R. P. Haugland, *Bioorg. Med. Chem. Lett.*, 1998, **8**, 3107–3110.
104 D. Chercka, S.-J. Yoo, M. Baumgarten, J.-J. Kim and K. Müllen, *J. Mater. Chem. C*, 2014, **2**, 9083–9086.
105 T. Jiang, J. Qin, J. Lin, X. Lin, W. Liu, Z. Xie, C. Redshaw, Z. Zhao and X. Feng, *ACS Appl. Mater. Interfaces*, 2025, **17**, 43339–43351.
106 Y. Liu, J. Zhang, X. Wang, Z. Xie, H. Zheng, S. Zhang, X. Cai, Y. Zhao, C. Redshaw, Y. Min and X. Feng, *J. Org. Chem.*, 2024, **89**, 3319–3330.
107 X. Wu, S. Ni, C.-H. Wang, W. Zhu and P.-T. Chou, *Chem. Rev.*, 2025, **125**, 6685–6752.
108 M. Rosenberg, K. R. Rostgaard, Z. Liao, A. Ø. Madsen, K. L. Martinez, T. Vosch and B. W. Laursen, *Chem. Sci.*, 2018, **9**, 3122–3130.
109 H. E. Gottlieb, V. Kotlyar and A. Nudelman, *J. Org. Chem.*, 1997, **62**, 7512–7515.
110 Z. Gryczynski and I. Gryczynski, *Practical Fluorescence Spectroscopy*, Taylor & Francis Group, 2019.
111 M. J. Frisch, G. W. Trucks, H. B. Schlegel, G. E. Scuseria, M. A. Robb, J. R. Cheeseman, G. Scalmani, V. Barone, G. A. Petersson, H. Nakatsuji, X. Li, M. Caricato, A. V. Marenich, J. Bloino, B. G. Janesko, R. Gomperts, B. Mennucci, H. P. Hratchian, J. V. Ortiz, A. F. Izmaylov, J. L. Sonnenberg, D. Williams-Young, F. Ding, F. Lipparini, F. Egidi, J. Goings, B. Peng, A. Petrone, T. Henderson, D. Ranasinghe, V. G. Zakrzewski, J. Gao, N. Rega, G. Zheng, W. Liang, M. Hada, M. Ehara, K. Toyota, R. Fukuda, J. Hasegawa, M. Ishida, T. Nakajima, Y. Honda, O. Kitao, H. Nakai, T. Vreven, K. Throssell, J. A. Jr, J. E. Peralta, F. Ogliaro, M. J. Bearpark, J. J. Heyd, E. N. Brothers, K. N. Kudin, V. N. Staroverov, T. A. Keith, R. Kobayashi, J. Normand, K. Raghavachari, A. P. Rendell, J. C. Burant, S. S. Iyengar, J. Tomasi, M. Cossi, J. M. Millam, M. Klene, C. Adamo, R. Cammi, J. W. Ochterski, R. L. Martin, K. Morokuma, O. Farkas, J. B. Foresman and D. J. Fox, 2016, *Gaussian 16, Revision C.01*, Wallingford, CT.
112 T. A. Manz and N. G. Limas, *ChargeMol program for performing DDEC analysis, Version 3.5*, 2017, ddec.sourceforge.net.
113 S. Ito, F. J. White, E. Okunishi, Y. Aoyama, A. Yamano, H. Sato, J. D. Ferrara, M. Jasnowski and M. Meyer, *CrystEngComm*, 2021, **23**, 8622–8630.
114 Rigaku Oxford Difraction Ltd, Rigaku Corporation, Wroclaw, Poland, 2025, CrysAlisPro.
115 O. V. Dolomanov, L. J. Bourhis, R. J. Gildea, J. A. K. Howard and H. Puschmann, *J. Appl. Crystallogr.*, 2009, **42**, 339–341.
116 G. Sheldrick, *Acta Crystallogr. C*, 2015, **71**, 3–8.
117 G. Sheldrick, *Acta Crystallogr. A*, 2015, **71**, 3–8.
118 L. M. Peng, *Micron*, 1999, **30**, 625–648.
119 F. H. Allen and I. J. Bruno, *Acta Crystallogr. B*, 2010, **66**, 380–386.
120 D. N. Rainer and J. Hester, *CIVET – CIF Validation and Editing Tool*, Zenodo, 2026, DOI: 10.5281/zenodo.18178135.
121 S. Ito, S. Kikuchi, N. Morita and T. Asao, *Chem. Lett.*, 1996, **25**, 175–176.
122 E. M. Arnett, R. A. Flowers, R. T. Ludwig, A. E. Meekhof and S. A. Walek, *J. Phys. Org. Chem.*, 1997, **10**, 499–513.
123 CCDC 2524713: Experimental Crystal Structure Determination, 2026, DOI: 10.5517/ccdc.csd.cc2qr5c1.